Journal of
Marine Science and Engineering

MDPI

Article

Towards Estimating Probability of Fish–Turbine Encounter: Using Drifters Equipped with Acoustic Tags to Verify the Efficacy of an Array of Acoustic Receivers

Brian G. Sanderson [1,*], Richard H. Karsten [2] and Daniel J. Hasselman [3,*]

[1] Acadia Centre for Estuarine Research, Acadia University, Wolfville, NS B4P 2R6, Canada
[2] Department of Mathematics and Statistics, Acadia University, Wolfville, NS B4P 2R6, Canada; richard.karsten@acadiau.ca
[3] Fundy Ocean Research Center for Energy, Halifax, NS B3J 3N5, Canada
* Correspondence: bxs@bellaliant.net (B.G.S.); dan.hasselman@fundyforce.ca (D.J.H.); Tel.: +1-902-697-2592 (B.G.S.); +1-902-406-1166 (ext. 7) (D.J.H.)

Abstract: An area has been designated for demonstrating the utility of marine hydrokinetic turbines in Minas Passage, Bay of Fundy. Marine renewable energy may be useful for the transition from carbon-based energy sources, but there is concern for the safety of fish that might encounter turbines. Acoustic receivers that detect signals from acoustically tagged fish that pass through the tidal demonstration area and the detection efficiency of tag signals might be used to estimate the likelihood of fish encountering marine hydrokinetic turbines. The method requires that tagged fish passing through the development area will be reliably detected by a receiver array. The present research tests the reliability with which passing tags are detected by suspending tags beneath GPS-tracked drifters. Drifters carrying high residency Innovasea tags that transmitted every 2 s were usually detected by the receiver array even in fast currents during spring tides but pulse-position modulation tags were inadequate. Sometimes very few high residency tag signals were detected when fast tidal currents swept a drifter through the receiver array, so increasing the transmission interval degrades performance at the tidal energy development area. High residency tags suspended close to the sea surface were slightly less likely to be detected if they passed by during calm conditions. Previously measured detection efficiencies were found to slightly overestimate the chances of a high residency tag carried by a drifter being detected as it passed by a receiver. This works elucidates the effectiveness with which acoustically tagged fish are detected in fast, highly turbulent tidal currents and informs the application of detection efficiency measurements to calculate the probability that fish encounter a marine hydrokinetic turbine.

Keywords: acoustic tag; verify; detection efficiency; tagged drifter; tidal energy; MHK turbine; fish–turbine encounter; acoustic telemetry

Citation: Sanderson, B.G.; Karsten, R.H.; Hasselman, D.J. Towards Estimating Probability of Fish–Turbine Encounter: Using Drifters Equipped with Acoustic Tags to Verify the Efficacy of an Array of Acoustic Receivers. *J. Mar. Sci. Eng.* **2023**, *11*, 1592. https://doi.org/10.3390/jmse11081592

Academic Editors: Louise Kregting, Nicholas Baker-Horne and Rosemary Norman

Received: 30 June 2023
Revised: 31 July 2023
Accepted: 11 August 2023
Published: 14 August 2023

1. Introduction

There has been, and continues to be, a substantial effort to develop marine renewable energy (MRE) in order to address the effects of climate change and ensure a transition from carbon-based energy sources that is both sustainable and environmentally benign [1]. In Minas Passage, Bay of Fundy, tidal currents can exceed 5 ms^{-1} and that raises the possibility that marine hydrokinetic (MHK) turbines [2,3] might be used to generate electricity from the kinetic energy of the tides, thereby offsetting Canadian carbon emissions [4,5]. An area has been designated and equipped for tidal energy demonstration (TED) adjacent to the northern shore of Minas Passage, Bay of Fundy, Canada (Figure 1). The installation of MHK turbines is subject to assessing and mitigating potential harm to marine animals (*Canadian Environmental Assessment Act*, *Fisheries Act*, *and Species at Risk Act*) [6]. There is particular concern for local populations of various fish species that are found in the

region [7–9]. For example, a local population of striped bass *(Morone saxatilis)* that spawns in the Shubenacadie River [10], Atlantic sturgeon *(Acipenser oxyrhinchus)* from the Saint John River stock [11], and inner Bay of Fundy Atlantic salmon *(Salmo salar)* that were once abundant but are now supported by local hatchery stocking programs [12].

Acoustic telemetry provides a means to tag individuals belonging to a specific population and measure how frequently they pass through the TED area. If an acoustic receiver is placed within the TED area and it detects an acoustically tagged fish, then there is a distribution of positions about the receiver where the fish might be, and the distribution can be estimated if we know the detection efficiency of a signal from the acoustic tag. Measurements of detection efficiency, ρ, enable detections of tagged fish to be converted into an estimate of abundance [13]. When the current is fast, tagged fish move with the water to a first approximation [14], so the flux of tagged fish can be estimated. Thinking of the receiver as a proxy for where an MHK turbine might later be deployed, the flux of tagged fish passing through the area swept by MHK turbine blades is an Eulerian formulation [15] from which we can calculate the probability that an individual fish will encounter a turbine. This probability of encounter is only an upper limit on the probability of harm. A fish that encounters an MHK turbine might avoid dangerous interaction or may even be struck by a turbine blade but not be harmed [16,17], but presently, there is little prospect of measuring avoidance behavior and strike survivability at the TED area in Minas Passage [18].

Detection efficiency, $\rho(r, s)$, has been measured in the TED area as a function of range, r, from tag to receiver and signed current speed, s ($\pm$ on flood/ebb tides) [13]. These measurements were made using Innovasea high residency (HR) tags that were detected by Innovasea HR2 receivers. Both tags and receivers were moored near the seafloor, and there were indications that signal paths were sometimes blocked by variable bathymetry. The present work will more definitively demonstrate signals blocked by variable bathymetry. In Minas Passage, MHK turbines have been deployed, and are expected to be deployed, well clear of the seafloor, and many of the fish species of concern are known to also swim well clear of the seafloor in the TED area [10,11,19]. The present work addresses, therefore, a pressing need to verify the extent to which the previously measured detection efficiency [13] is applicable to the detection of tags that are located higher in the water column.

In order for later work to rigorously estimate the probability of fish–turbine encounter [20], it is necessary to presently verify that the number of signals detected during the time interval in which a tagged fish passes by a receiver will be consistent with the number estimated from detection efficiency that was measured using a tag moored to the seafloor [13]. Such measurements cannot be made using tagged fish because there is no way to know when a tagged fish passed the receiver array without being detected. Based on previously published work [14,20], to a good approximation, in the fast currents of Minas Passage, tagged fish move like drifters. To be representative of a tagged fish, the following work deployed HR tags suspended beneath GPS-tracked drifters in order to verify that they were detected by near-seafloor receivers in a way that was consistent with previously measured detection efficiency [13] and their track. Given that the species of interest can be found at different levels within the water column [10,11,19], each drifter suspends four tags at different subsurface depths.

Two measurement strategies were used. First, short-term drifts (STDs), where the tagged drifter was repeatedly released upstream and collected downstream of HR2 receivers in order to obtain many measurements in the TED area (Section 2.2). Second, long-term drifts (LTDs), where drifters were released onto a quasi-stable trajectory [14] and not recovered until many days later (Section 2.3). The quasi-stable trajectory [14] was chosen to efficiently obtain many measurements over HR2 receivers moored to the south of the TED area.

Conventionally, detection efficiency has been measured using acoustic tags and receivers that are at fixed positions [13,21,22]. Although seldom stated, such measurements give a strictly Eulerian formulation for detection efficiency. Such measurements of detection efficiency are related to the probability of detecting a tagged fish as it passes fixed receivers.

The presently obtained measurements provide a Lagrangian formulation [15] to directly obtain the probability of detecting a moving tag as it drifts by a receiver on a specific track. It should be stressed that the analysis presented below is only of acoustic tags attached to drifters. However, since the ultimate goal is to apply this work to detecting tagged fish moving through Minas Passage (see [14]), the analysis is discussed in terms of its relevance to tagged fish.

2. Materials and Methods

The volcanic plateau of the TED area in Minas Passage (Figure 1) is presently favored for future installations of both gravity-based MHK turbines and also for MHK turbines mounted to a floating platform [2]. The field program was designed to minimize the possibility of equipment, particularly drifters, becoming entangled with a non-operational OpenHydro turbine at the position marked by a circled cross in Figure 1a.

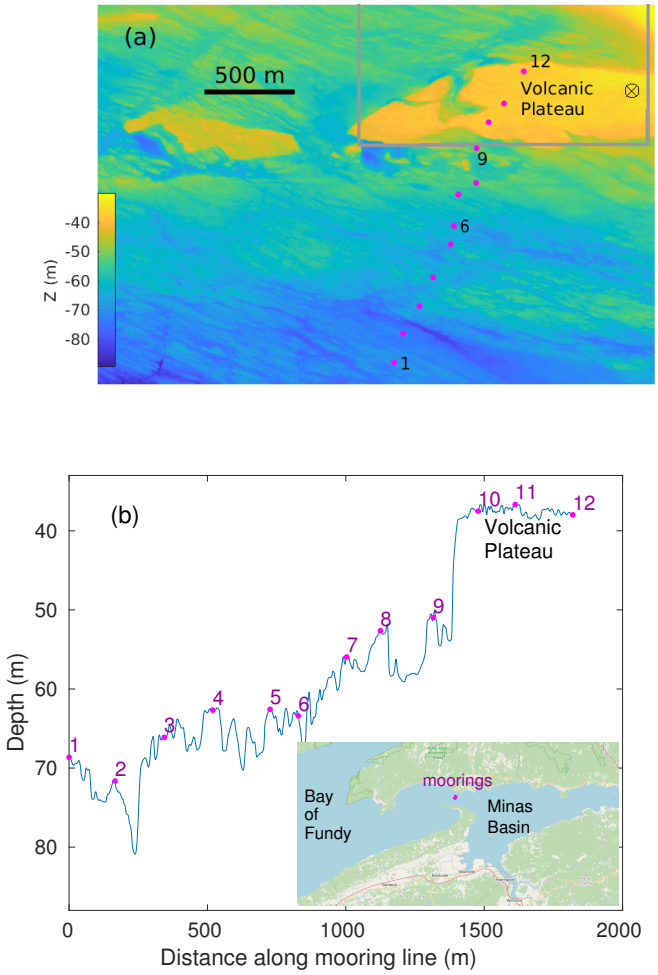

Figure 1. Mooring layout in Minas Passage. (**a**) Plan view shows moorings 1 through 12 and the TED area (gray box). (**b**) Depth profile along the mooring line. Inset shows location of the moorings within Minas Passage, Bay of Fundy.

2.1. Moorings

Twelve mooring sites were chosen so as to deploy an array of acoustic receivers on high ground along a line that was oriented approximately orthogonal to the flood tide (Figure 1). Mooring sites 1–8 monitored tagged drifters that crossed a line to the south of the TED area. Sites 10–12 were on the volcanic plateau, and site 9 was in deeper water off the edge of the plateau. Jointly, sites 9–12 are considered to monitor the TED area. Whereas

the volcanic plateau is relatively flat, the area to its south is characterized by highly variable bathymetry (Figure 1b).

All moorings consisted of a 240 kg chain link that served as an anchor to which a SUBS-Model A2 float (Open Seas Instrumentation Inc., Musquodoboit Harbour, Canada) was tethered by a 3 m riser chain. Each SUBS carried an acoustic release and an HR2 receiver within its streamlined hull and an Innovasea VR2W-69kHz receiver mounted symmetrically behind its tail fin. The HR2 receivers were set to transmit 143 dB HR signals every 25–35 s and record tilt and water temperature every 10 min. At moorings 9–12, a V9 tag was mounted to the top of the SUBS tail fin, and it transmitted a 170 kHz HR signal with a manufacturer-specified transmission interval of 1.8–2.2 s. Actual transmission intervals for the V9 tags were 1.800–2.1750 s with an average of 1.9875 s. V9 tags at moorings 9 and 10 operated throughout the deployment period but the tags at moorings 11 and 12 failed on 16 July 2022 and 1 August 2022, respectively.

Moorings were deployed during 5–6 May 2022. The SUBS at mooring 3 re-surfaced immediately following deployment. The hull of the SUBS was deformed and scuffed, and the attachment for its mooring assembly (anchor and riser chain) had sheared from the fiberglass strong-back that held the acoustic release. The most likely explanation was that the anchor of mooring 3 had fallen into a deep crevasse that was too narrow for the SUBS to follow.

An initial estimate of each mooring deployment position was obtained from the deployment vessel's GPS at the time that the mooring was released overboard from the stern. The estimate of the mooring position had uncertainty due to the vessel's GPS being located 10.4 m forward of the stern and vessel heading being variable and uncertain when the mooring was released. To refine the deployment position, Columbus V990 GPS loggers were placed on each side of the stern deck, and another was used to mark the time at which a mooring was released overboard.

Of the 11 moorings successfully deployed, 10 were recovered on 6 September 2022 with receivers in good working order. The acoustic release at mooring 5 did not respond to the deck unit. On 18 September 2022, the SUBS from mooring 5 washed ashore near Harbourville, Nova Scotia, and was promptly recovered with its chain riser still attached to the acoustic release. The VR2W receiver had broken off the SUBS and was lost, but the HR2 was still attached and its data were successfully downloaded. The last time the HR2 at mooring 5 detected HR signals from neighboring moorings was 13 August 2022 00:55:41, so it must have become detached from its anchor weight at about that time.

HR2 clocks were set relative to UTC shortly before mooring deployment and shortly after mooring recovery when data were downloaded. The clock sets enable linear clock skew to be corrected by Innovasea software as a part of the data download. Over the deployment period for the 11 HR2 receivers that were recovered, linear time offsets ranged from −172 s to 161 s, with a mean of −80 s and a root mean square of 132 s. Provided a pair of HR2 receivers could detect each other's HR transmissions, their separation range was calculated, and their clocks were synchronized to each other [13].

2.2. Short-Term Drifts (STDs)

Short-term drifts (STDs) comprised many (n = 62) brief drifts during spring flood tides in order to determine how well HR tags could be detected as they passed over the array of HR2 receivers deployed in the TED area. A pole float was convenient for quick and easy handling during drifter deployment and recovery.

A Columbus V-990 GPS logger was fixed to the top of the pole float and logged GPS positions every second. Beneath the sea surface, the pole-float drifter was configured with four V9 170 kHz HR tags placed at 3 m, 8 m, 16 m, and 26 m subsurface depths. The V9 tags transmitted an HR signal every 1.8–2.2 s. An HR2 receiver was suspended at 21 m depth with its hydrophone sensor pointing downwards and configured to record temperature and instrument tilt every 60 s. A V16 69 kHz PPM tag was attached at 27 m subsurface and

transmitted every 10 s. A 4.7 kg lead weight was attached 28.5 m subsurface to vertically align equipment within the water column.

The STDs were conducted using a 6 m rigid-hull inflatable boat (RHIB) that was fitted with a 110 hp outboard engine. Experiments were conducted during relatively calm weather (forecast wind either light or up to 5 ms^{-1} and directed with the tidal current) and timed to coincide with large spring tides so tests could be conducted during elevated tidal current speeds. Although the pole-float drifter was not drogue, the fast tides and light winds ensured that drifter movement was a good approximation to that of the top 28 m of the water column. Most measurements were made on and about peak flood tide because these were the conditions for which we had least confidence in the reliability of the previously measured detection efficiency [13].

The operating procedure was to deploy the drifters about 800–1000 m upstream of the moored receivers and begin recovering them after they had drifted 600 m past the receivers. Deployment was swift and easy, so drifters were almost always safely set and the research vessel's engine turned off before the drifter had approached within 500 m of the moorings. Recovery was laborious and time-consuming, which limited how many drift tracks could be achieved in a day. The onset of wind or fog shortened some working days. Drifts were conducted on 13 June (n = 16), 15 June (n = 15), 16 June (n = 6), 17 July (n = 16), and 18 July (n = 9).

The HR2 suspended beneath the STD operated over short time periods, and clock sets gave linear time offsets of −5.5 s over the June experiments and −3.9 s over the July experiments. When signals from the drifting HR2 were detected by moored HR2 receivers, it was possible to synchronize clocks between the moorings and drifter.

2.3. Long-Term Drifts (LTDs)

The long-term drifters were designed so they could be tracked remotely using either a web browser or an application (app) on a smartphone or tablet. Drifters suspended HR tags and were usually deployed so that they would settle onto quasi-stable trajectories that passed over the moored HR2 receivers [14]. When drifters went off track, they could be located using the app and recovered or redeployed using the abovementioned RHIB.

Three long-term drifters were constructed. Each drifter consisted of a surface float, a 1.8 m by 2.45 m window shade drogue centered at a 6.3 m depth, and a long trailing line that held instruments and terminated at a 7 kg steel weight. The surface float was constructed from 38 mm ABS pipe and standard plumbing fittings with flotation fashioned from 50 mm boards of extruded polystyrene foam. Batteries and electronics were assembled on a length of ABS and slid into the ABS pipe.

The electronics package consisted of a Tractive® GPS LTE dog tracker, a Columbus V-990 GPS logger, and a buck converter that supplied 5V DC via USB connectors. Tractive® enabled remote tracking but provided position measurements at irregular intervals, ranging from a few minutes to many hours depending upon the cellular network. Columbus V-990 logged GPS positions every second but had to be physically recovered to download data. The buck converter could provide 5V-USB to instruments from an 8–24 V D-cell stack.

The Columbus GPS logger prematurely stopped logging during some early LTD drifts because an inappropriate USB cable was used to connect with the buck converter. This problem was solved by using the USB cable that was sold with the Columbus GPS logger.

2.4. Tidal Current and Surface Elevation

Using drifters that carry both acoustic tags and GPS loggers has the advantage of providing current information that coincides with the detection of tags by moored receivers. Nevertheless, the detection efficiency that we aimed to test was formulated as a function of current speeds that were calculated using the FVCOM hydrodynamic model [4,13,23]. Tidal currents and sea surface elevation have been simulated for the Bay of Fundy, and the present work utilizes values saved at 10-min intervals at each of the mooring positions.

Modeled tidal elevation was used to obtain the vertical part of tag–receiver separation so that the slant range could be calculated.

3. Results

3.1. STD Tracks and FVCOM Current

A total of 62 drift tracks were made during large spring tides: 37 during June and 25 during July flood tides. Figure 2 shows the portion of each track that was kept for analysis. Six tracks were measured on the 15 June ebb tide, and the remainder were measured during flood tides. Ebb tide tracks are more zonal than flood tracks, consistent with centrifugal effects as the flood tide enters Minas Passage [14]. Except near the turn of the tide, drifter tracks take a fairly straight path across the line of moorings. Smaller-scale variability in the track is probably associated with flow over variable bathymetry (Figure 1) and turbulent "boils", which intensify with tidal current speed.

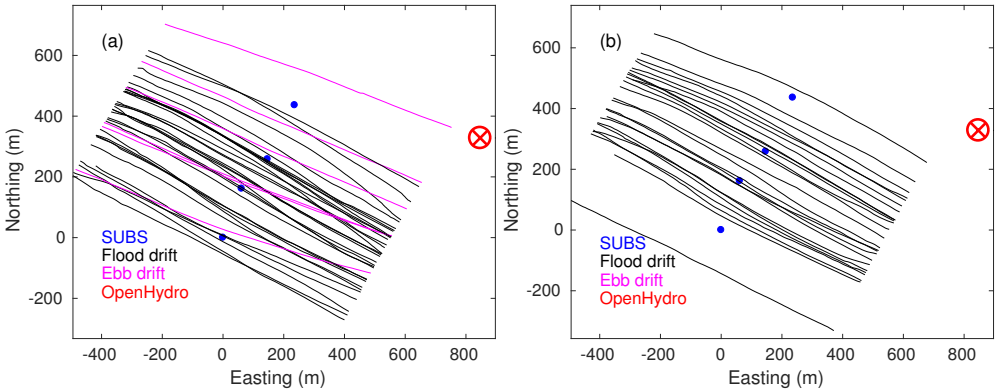

Figure 2. STD tracks. Positions of moorings 9–12 are marked with blue dots. Black lines show flood tracks. Ebb tracks are magenta. Tracks were measured on (**a**) 13, 15, and 16 June 2022 (n = 37) and (**b**) 17 and 18 July 2022 (n = 25).

HR signals are only expected to be detected in the mid portion of the plotted tracks, near where they most closely approach a moored HR2 receiver (Figure 2). With that in mind, each track can be characterized relative to a mooring by the time of closest approach, t_{ca}; the slant range of closest approach, r_{ca}; and signed drifter speed, s_{ca}, at the time of closest approach. Signed drifter speed is defined herein as positive on the flood tide and negative on the ebb tide. Drifter velocity was computed from drifter positions 10 s before and after t_{ca}.

Previously measured detection efficiency [13] was expressed as a function of signed current speed at the position of the detecting mooring, so it is germane to compare drifter current with FVCOM simulated current. For each of the 62 drifts, the signed current speed, s_{FV}, was obtained from FVCOM simulated current at the mooring, m_{ca}, most closely approached and at the time of closest approach. Regressing s_{FV} against the corresponding s_{ca} gives:

$$s_{FV} = a s_{ca} + b, \quad (1)$$

where $a = 0.87$ (95%CI 0.84–0.89), $b = 0.14$ ms^{-1} (95%CI 0.04–0.25), and R-square is 0.99. Caution is warranted because few ebb tides were measured, but it is quite clear that drifters move faster than FVCOM simulations would suggest during flood tide in the TED area. FVCOM currents were vertically averaged over the water column and the pole-float drifter extended from about 1.5 m above the sea surface to a depth of about 29 m.

3.2. Mooring Separation, Synchronization, and Depth

Figure 1 plots the estimated deployment positions for moorings and shows the depths at these positions. There is a possibility that moorings may move during the experiment due to drag and lift forces exerted on the SUBS. A change in the separation of moorings

can indicate the extent of mooring movement, as can a change in depth and a change in HR signals reflected from a nearby object [13].

When two HR2 receivers can detect each other's transmissions, then it is straightforward to calculate their separation and synchronize their clocks [13]. Similarly, an HR2 can be treated as an inverted echosounder in order to measure the distance below the sea surface, which must then be detided to find depth [13]. HR2 separation ranges were essentially constant with respect to time for each of the following pairs of moorings: 1–2, 4–5, 5–6, 6–7, and 9–10 (Table 1). Furthermore, HR2 depths at sites 1, 2, 4, 5, 6, 7, 9, and 10 did not substantially change with time, so it is safe to conclude that these moorings did not move to any meaningful extent (except for mooring 5 breaking free on 13 August). Moorings at sites 8, 11, and 12 moved, but the depth changes were not great.

Table 1. Separations between moorings.

Mooring Pair	Separation (m)	Dates (2022)	Depths (m)
1–2	166	7 May–6 September	66.3, 69.2
4–5	209.5	7 May–14 May	59.3, 59.9
4–5	209.4	14 May–13 August	60.0, 59.9
5–6	106	7 May–13 August	59.9, 61.1
6–7	206	7 May–6 September	61.1, 52.8
7–8	123	7 May–14 June	52.8, 49.7
7–8	132	18 June–17 July	52.8, 49.6
7–8	135	19 July–12 August	52.8, 50.4
7–8	137	13 August–6 September	52.8, 50.7
8–9	190	7 May–12 May	50.0, 48.4
8–9	193	14 May–14 June	50.0, 48.4
8–9	200	19 June–17 July	49.6, 48.4
8–9	206	19 July–6 September	50.5, 48.4
9–10	182	7 May–6 September	48.4, 34.8
10–11	133	7 May–15 May	34.8, 34.1
10–11	152	19 May–14 July	34.8, 34.9
10–11	174	17 July–6 September	34.8, 35.7
11–12	211	7 May–15 May	34.1, 34.9
11–12	232	21 May–14 July	34.9, 34.8
11–12	230	17 July–6 September	35.7, 34.9

Pairs of HR2 receivers (sites 9–10, 10–11, and 11–12) were synchronized. Given that all adjacent pairs could be synchronized, it is straightforward to obtain the time corrections that will synchronize HR2 receivers at sites 10, 11, and 12 with the HR2 at site 9 (Figure 3). Usually, the dominant term for the nonlinear time correction is quadratic, so we were surprised to observe an abrupt 1 s jump for the HR2 clock at site 12. Site 12 is nearest to a highly turbulent area associated with Black Rock, a small island close to the northeast corner of the TED area. It is possible that the SUB at site 12 became unstable and crashed into the seafloor, perhaps causing an interruption of the power supply. Alternatively, Innovasea suggested that infrequent 1 s clock jumps were a feature of some early HR2 models, but changes to firmware are thought to have eliminated that problem. Regardless, this clock jump cannot be dismissed as "a bad data point" because all the following estimates of time correction are consistent, and they are all calculated from independent measurements.

The time corrections in Figure 3 are two orders of magnitude smaller than the linear clock skew that Innovasea software automatically corrects for when data are downloaded. Synchronizing an array of HR2 receivers is useful if that array were to be used for localizing the position of a passing tag, but this is not sufficient to relate HR signals detected by moored HR2 receivers to the concurrent position of the STD.

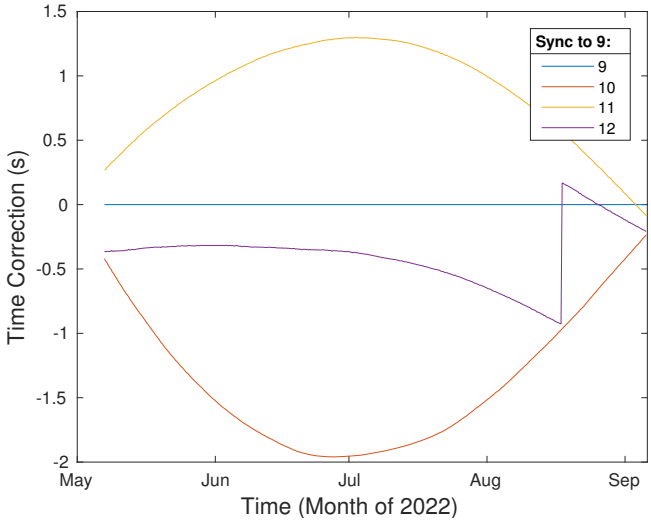

Figure 3. Nonlinear offset to synchronize receivers at stations 9 through 12 to the receiver at station 9.

3.3. Synchronizing Moored HR2 Receivers to the STD

The requirement is to use time as a parametric variable in order to match a detected signal to the concurrent position of a drifter. Drifter positions are synchronized to UTC, so the task is to synchronize the array of HR2 receivers (at moorings 9–12) to UTC. Our method requires an assumption that will turn out to be justified by the outcome.

Short-term drifts were conducted for a few days in June and a few days in July. The HR2 carried by the drifter operated over short periods between clock sets, and the corrections for linear clock skew were only -5.5 s and -3.9 s for the June and July experiments, respectively. Assume for a moment that the uncorrected nonlinear drift would have been much smaller than linear clock skew so that the HR2 suspended beneath the drifter records detected HR signals to within a fraction of a second of UTC. The suspended HR2 detects the HR tag suspended 5 m below it very well. Drifts 11 and 31 occurred within the first pair of time sets (i.e., June experiments), and during these drifts, the HR2 at mooring 9 also detected the suspended tag. The intervals between the tag transmissions are variable, so by lining up the pattern of detection times measured by the HR2 on the drifter with the pattern of detection times measured by the HR2 at mooring 9, we can synchronize the HR2 at mooring 9 to the HR2 suspended by the pole float. In this way, all clocks become synchronized to UTC within a fraction of a second. (Signal time of travel is small enough to be ignored for present purposes). Drifts 54 and 55 can similarly be used to synchronize HR2 receivers for the July experiments.

Table 2 shows how much the HR2 at mooring 9 needed its time advanced in order to match the times of the HR2 attached to the pole float/UTC. The time advance is small compared with the linear clock skew (root mean square, 132 s) over the duration of HR2 moorings, so it was fair to assume that data downloaded from the HR2 suspended on the drifter would have matched UTC to within a fraction of a second. It is noteworthy that Table 2 indicates nonlinear time drift that is common to the four HR2 receivers and that this is large when compared with the differences between receivers (Figure 3). More relevant for our present purpose, not accounting for the time increment in Table 2 would correspond to a 4 ms^{-1} current causing about 60 m error when aligning drifter position with times that signals are detected.

Table 2. Time corrections to add to the HR2 at mooring 9 in order for it to match the HR2 receiver suspended below the pole-float drifter.

Drift Number	Date	Time Correction (s)
11	13 June 2022	16.75
31	15 June 2022	16.45
54	18 July 2022	15.5
55	18 July 2022	15.5

Figure 4 shows HR signals detected at various ranges along drift tracks. Upwards propagating signals travel from the moored tag to the drifting HR2 and downwards signals from the 25 m tag on the drifter to the moored HR2. With a 3.46 ms^{-1} flood current, both upward and downward HR signals are detected over many ranges. When the flood current is 4.92 ms^{-1}, the signals are detected at relatively small ranges (up to 69 m in Figure 4b). Using (1), the corresponding FVCOM speeds would be 3.15 ms^{-1} and 4.42 ms^{-1} for which interpolating from earlier work [13] gives detection efficiencies of 0.75 and 0.09 in a 75 m range, respectively. Consistent with low detection efficiency and reasonably accurate synchronization to UTC, most detected signals are clustered near the range of closest approach in Figure 4b.

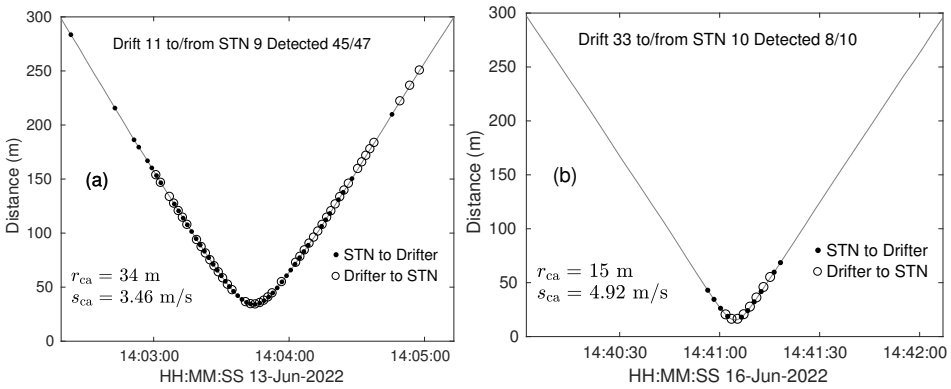

Figure 4. Signals detected as a function of distance and range along STD tracks. (**a**) Many signals are detected at moderately high current speed. (**b**) Fewer signals are detected at very high current speed.

3.4. Number of STD Tracks Detected by the Receiver Array

Of the tagged fish that pass through the TED area, it is of particular interest to know what fractions are expected to be detected by the moored receiver array. This question can be addressed by asking how many of the tagged STD drifts were detected. Given that the STD carried HR tags at four subsurface depths, we can also address the question as to whether or not the swimming depth of a tagged fish matters for signal detection.

STD tracks were always detected when current speed was low, so let us select the 45 fast tracks that had $|s_{ca}| > 3.5$ ms^{-1} for more detailed analysis. For each drift, we counted the number of times, N_{DA}, that each tag was detected by the array of moored HR2 receivers. Thus, for a given tag, we construct an $I = 45$ element vector $\vec{N}_{DA} = (N_{DA1}, N_{DA2}, \cdots, N_{DA45})$ containing the number of times the tag was detected during each of its 45 drifts. Counting the number of drifts for which the array detected a specific tag at least once gives the number, N_{PEDA}, of passing events detected by the array

$$N_{\mathrm{PEDA}} = \sum_{i=1}^{I} \min(N_{DAi}, 1), \tag{2}$$

as recorded for each tag in the first row of Table 3. Of the 45 fast drifts that passed the HR2 array, 44 were on the flood tide.

Fewer drifts were detected by a tag nearer the sea surface (Table 3). In part, this may be because the HR2 receivers were on the seafloor, so a tag is a little further away if it is near the sea surface. During spring flood tides, visual observations have been made of tidal eddies that generate localized, breaking surface waves near strong convergence at the edge of the eddy. It is possible that bubbles are entrained well into the water column and that these may make it more difficult for near-bottom receivers to detect near-surface tags. Another mechanism is the possibility that an HR signal taking a direct path might interfere with its reflection from the sea surface. The time lag between direct and reflected paths is

$$\delta t = \frac{1}{c}(\sqrt{H^2 + (D_X + D_R)^2} - \sqrt{H^2 + (D_X - D_R)^2}), \quad (3)$$

where H is the horizontal distance from a transmitter at depth D_X to a receiver at depth D_R. Considering the typical values for the tag closest to the sea surface ($H = 50$, $D_X = 3$, $D_R = 34$) gives a 2.2×10^{-3} s time lag, so the reflection and direct signal will partially overlap in the received signal, given the 6×10^{-3} s duration of an HR signal. HR tags encode identity using a sequence of phase shifts [13], and signals are not recorded as detected unless they have also been identified.

Table 3. Out of the 45 fast ($|s_{ca}| > 3.5$ ms^{-1}) STD passing events, we tabulate the number of passing events (N_{PEDA}) for which a tag at a given depth was detected by the HR2 array.

τ (s)	3 m Tag	8 m Tag	16 m Tag	26 m Tag
2	39	38	42	44
4	36	37	40	42
8	31	34	34	39
16	22	25	26	34
32	14	17	17	21
64	7	10	10	13

Each of the four tags had an average transmission interval of $\tau = 2$ s. If the tags had been programmed for a T s transmission interval, then the number of transmitted signals would be reduced by a factor of τ/T, so the expected number of detected signals, ${}_eN_{DAi}$, during the ith drift (past the array) would be reduced by the same factor

$${}_eN_{DAi} = \frac{\tau}{T} N_{DAi}, \quad (4)$$

and the expected number of detected drifts would be

$${}_eN_{PEDA} = \text{nint}\left(\sum_{i=1}^{I} \min({}_eN_{DAi}, 1)\right). \quad (5)$$

As the transmission interval is increased, successive rows in Table 3 show that fewer drifts will be detected by the receiver array. With $\tau = 2$ s, about 15% of near-surface tags will not be detected as they drift by in >3.5 ms^{-1} currents but, at greater depth, only 2–6% would not be detected. Thus, the great majority of fish carrying $\tau = 2$ s tags would be detected, and a first-order estimate of the probability of encounter might be achievable and might be prorated for the small fraction that passes by without being detected. Reducing τ is expected to improve performance, but further measurements would be required in order to quantify by how much.

The STD experiments included a 27 m subsurface V16 69 kHz PPM tag that transmitted every 10 s. Due to mistakes in the field, this tag was only turned on for 55 of the 62 drifts. Although the V16 tag was powerful (158 dB), it was only detected for 29 of the 55 tracks, and these tracks were usually slow $1.6 < |s_{ca}| < 4.3$ ms^{-1} (mean 3.3 ms^{-1}). The 69 kHz PPM tag was not detected for 26 fast tracks where current speeds were $4.3 < |s_{ca}| < 5.1$ ms^{-1} (mean 4.6 ms^{-1}). For the two STD tracks with $|s_{ca}| < 2$ ms^{-1}, the 69 kHz PPM tag was

detected by VR2W receivers at 8 and 9 of the 11 mooring locations. The detection of 69 kHz PPM tags at a great range was expected when current speed was low [24], and this strongly contrasts with the poor performance observed in fast currents. Usually, the interval between PPM signals is much larger than 10 s, for fear of interference when more than one tag is present. A transmission interval of 60 s would be more typical, and in this case, it should be expected that only 21 of the 55 passing tracks would have been detected. For measuring the probability of fish–turbine encounter, PPM tags are deemed inadequate in the TED area.

3.5. Comparison of Detection Efficiencies at the TED Area

The present line of moored HR2 receivers and tags can be used to obtain estimates of detection efficiency, which can be compared with those previously reported [13]. Previous measurements were sometimes called into question because there were good physical grounds for the possibility that variable bathymetry blocked signals, even though bathymetry and signal paths could not be sufficiently resolved to determine where the signal was blocked [13].

Figure 1b shows that moorings 8 and 9 are on high ground relative to the path between them. On the other hand, the path from moorings 9 to 10 is most certainly blocked by the edge of the volcanic plateau. To make a comparison between these paths, we consider how the HR tag at mooring 9 is detected by HR2 receivers at moorings 8 and 10. Figure 5a shows that from 19 July to 6 September, the detection efficiency along the 9–8 path was very similar to that previously obtained [13] by eliminating measurements that were thought to be blocked. There was some mooring movement at site 8, but similar results were obtained during other time intervals when separation between moorings 8 and 9 was stable (Table 1). If anything, when currents are slow, the signal detection is more efficient than had previously been measured. On the other hand, the obvious blockage caused by the edge of the volcanic plateau causes detection efficiency to be extremely poor for signals propagating from mooring 9 to mooring 10 (Figure 5b). These results provide a little more confidence in the detection efficiencies obtained by [13] and also indicate that they apply immediately to the south of the TED area.

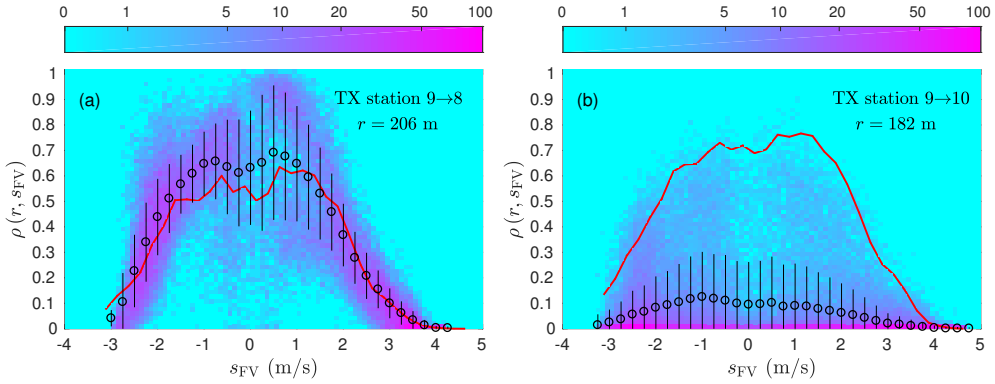

Figure 5. Average detection efficiencies are plotted as functions of s_{FV}, with black circles and lines indicating ± SD. Signals from the HR tag at mooring 9 are detected by (**a**) the HR2 at mooring 8, (**b**) the HR2 at mooring 10. For corresponding ranges, the red lines show detection efficiencies measured in 2022. The distribution of detection efficiencies calculated from 2 to minute intervals is shown using a logarithmic color scale. The distribution was normalized to a maximum value of 100 per ρ-s_{FV} bin.

The four SUBS used to monitor the TED area (i.e., moorings 9–12) carried an HR tag on the tail fin and an HR2 mounted inside the streamlined hull, so this enabled detection efficiency to be estimated as a function of FVCOM current, s_{FV}, when the range was about 1 m. Detection efficiency varied from 0.997 to 1.000 and, thus, can be considered effectively 1 for all current speeds observed at the TED area. This confirms the previous result [13],

which was based on more tenuous evidence (an HR signal with a fake identity) and a complicated line of reasoning.

3.6. Number of HR Signals Expected to Be Detected during a Passing Event at the TED Area

Define a *passing event* as a tagged drifter (or tagged fish) passing a moored HR2 receiver. For present purposes, passing events of interest result from the drifter (or fish) being advected by fast tidal currents. Tagged drifter measurements enable direct measurement of the number, N_D, of HR signals detected by a specific HR2 receiver during a passing event. In our study, the drifter tracks follow a straight line to a reasonable approximation (Figure 2), so $N_D(r_{\mathrm{ca}}, s_{\mathrm{ca}}, \tau)$.

We expect that an estimate N_E for N_D could be calculated from detection efficiency [13]. Let the position of the drifter relative to an HR2 be a function of time $(x(t), y(t), z)$, such that range from drifter to HR2 is also a function of time, $r(t) = \sqrt{x^2 + y^2 + z^2}$. Then, the number of HR signals that are expected to be detected during a passing event is found by integrating along the passing track as follows:

$$N_E(r_{\mathrm{ca}}, s_{\mathrm{ca}}, s_{\mathrm{FV}}, \tau) = \frac{1}{\tau} \int \rho(r(t), s_{\mathrm{FV}}) dt. \quad (6)$$

A comparison of N_E with N_D requires that the position of the moored HR2 receiver be accurately known. At the TED area, recall that only moorings 9 and 10 did not move (Table 1). For each of the tag-passing events, begin by comparing the number of HR signals detected by the array, N_{DA}, comprising receivers at moorings 9 and 10 with the number expected to be detected, N_{EA}. Summing over the 44 tracks that had $s_{\mathrm{ca}} > 3.5$ ms^{-1}, the number of HR signals detected from each tag, $\sum N_{DA}$, it is evident that near-surface tags are detected much less frequently than the deeper tags (Table 4). However, tag depth has only a small effect on the number of signals expected to be detected, $\sum N_{EA}$, by the array. The above calculation of N_E, and thence N_{EA}, does not take into account the possibility of interference due to the signal being reflected from the sea surface. These three facts indicate that interference by reflected HR signals (3) can reduce the chances that a near-surface tag will be detected (e.g., Table 3).

It is notable that the expected number of detected signals is greater than the number actually detected (Table 4). Such overestimation might happen because the range testing [13] obtained few measurements during the fastest currents and because errors in FVCOM modeling can sometimes assign detected signals to fast currents when they were actually detected in slow currents for which detection efficiency is higher. Furthermore, some signal paths to the HR2 at mooring 9 may have been blocked by the edge of the volcanic plateau (Figures 1b and 5b).

Table 4. Comparison of number of signals detected by an array, N_{DA}, with number expected, N_{EA}, at each tag depth. Measurements are from 44 fast flood drifts at the TED area. N_{PEDA} is the number of passing events detected by the array, and N_{PEEA} is the number that was expected to be detected. The rows labeled ${}_{0.78}N_{PEEA}$ and ${}_{0.43}N_{PEEA}$ show values of N_{PEEA} obtained when N_{EA} was rescaled by factors of 0.78 and 0.43, respectively.

	2.25 m Tag	**9 m Tag**	**19 m Tag**	**28 m Tag**
$\sum N_{DA}$	127	185	214	270
$\sum N_{EA}$	295	308	325	344
N_{PEDA}	26	28	28	26
N_{PEEA}	33	33	33	33
${}_{0.78}N_{PEEA}$	32	32	33	33
${}_{0.43}N_{PEEA}$	29	30	31	31

Of the 44 passing events, we can use (2) to determine the number of passing events that were detected by the array (N_{PEDA}), and similarly, the number of passing events that were expected to be detected by the array

$$N_{\mathrm{PEEA}} = \sum_{i=1}^{45} \min(N_{EAi}, 1). \tag{7}$$

Comparing N_{PEDA} with N_{PEEA} (Table 4) shows that fewer tracks were detected than expected. Note that this cannot be accounted for by simply adjusting the values of N_{EA} to reflect the depths of the drifting tags. Rescaling N_{EA} by a factor of 0.78 (consistency with the 28 m tag) did not bring the expected number of detected tracks into alignment with the measured number. Even rescaling N_{EA} by a factor of 0.43 (consistency with the 2.25 m tag) does not sufficiently change the expected number of detected tracks.

In addition to "downward" paths from the drifting tags to the moored HR2 receivers, there were also "upward" paths from the moored tags to the HR2 receiver that was suspended at a 21 m depth (5 m above the lowest tag suspended by the drifter). Let us now consider the upward paths from moorings 9 and 10 along with downward paths from the two lowest tags on the drifter to moorings 9 and 10. Selecting the 44 passing events with $s_{\mathrm{ca}} > 3.5$ ms^{-1}, it is confirmed that N_E generally declines with increasing r_{ca} (Figure 6), although there is a good deal of scatter, some of which might be associated with s_{ca} varying from track to track. Each downward path had a similar upward path.

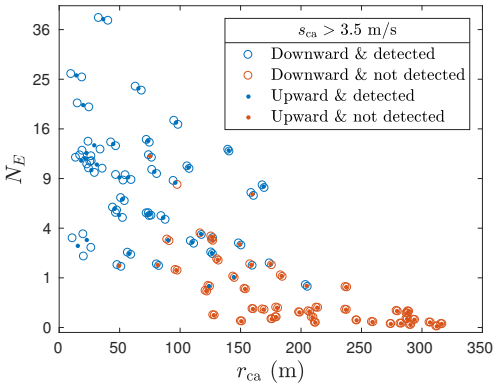

Figure 6. The expected number of detected signals, N_E, declines with increasing slant range of closest approach, r_{ca}. Only the 44 STD tracks with $s_{\mathrm{ca}} > 3.5$ ms^{-1} are included.

Figure 6 stratifies N_E into those for which the corresponding measurement obtained $N_D > 0$ (blue) and those for which $N_D = 0$ (red). HR2 receivers did not detect HR signals when $\mathrm{nint}(N_E) = 0$, but there are a problematic number of occasions when $\mathrm{nint}(N_E)$ is considerably greater than 1, and yet, no signals were detected by the HR2 receiver. (The operator nint(x) gives the nearest integer to x). To see the issue more clearly, Figure 7 plots the number of detected signals, N_D, as a function of the number expected $\mathrm{nint}(N_E)$. Clearly, sometimes more signals are detected than expected and sometimes fewer. One might expect that sometimes no signals are detected when several are expected, but it is very odd that it never happens that a few signals are detected against an expectation that none are expected. Rescaling N_E so that $\sum N_E = \sum N_D$ (e.g., Table 4) made no difference. This unexpected asymmetry of Figure 7 points to something being wrong about the calculation made using (6).

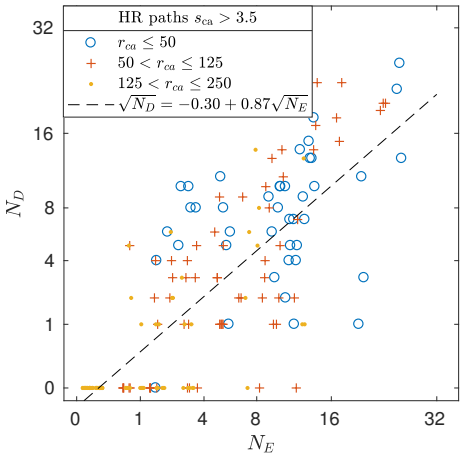

Figure 7. Number of detected signals for STD passing events plotted as a function of the number expected.

Equation (6) uses an empirical functional form $\rho(r, s_{\mathrm{FV}})$ for detection efficiency in the sense that each black circle in Figure 5 represents an average of a cloud of many detection efficiencies calculated from many 2-min time intervals. Rather than plot each 2-min detection efficiency, Figure 5 uses color to represent their distribution on the ρ–s_{FV} plane. Clearly, detection efficiency is a fluctuating variable relative to its long-term average. If s_{FV} accurately resolved the local current, including turbulent eddies, then some portion of the variability in Figure 5 would likely be resolved within the function, $\rho(r, s_{\mathrm{FV}})$, but there would still be variability about $\rho(r, s_{\mathrm{FV}})$ because the local sound level is only related to current speed in a statistical sense. In reality, FVCOM does not perfectly model tidal currents, let alone accurately resolve turbulent eddies.

Representing the fluctuations of detection efficiency as $\rho'(t)$ gives

$$N_E + N'_E = \frac{1}{\tau} \int \rho(r(t), s_{\mathrm{FV}}) + \rho'(t) dt. \tag{8}$$

Both ρ' and N'_E average to zero for a sufficiently large ensemble, but tag signals may only be detected for 30 s (or less) during a passing event (Figure 4). A fluctuation, $\rho'(t)$, cannot be expected to be totally independent of the fluctuation, $\rho'(t - \delta t)$, shortly before. Such correlation has implications for the detection of passing events. Fluctuations in $\rho(r, s_{\mathrm{FV}})$ will not change the total number of signals detected over a large number of passing events, but correlations will distribute these detections differently among passing events. Where correlations cause a drifter track to be detected more often than for uncorrelated fluctuations, it will still be counted as the detection of a single passing event. Where correlations cause a drifter track to be detected fewer times, a passing event might be shifted from being detected to not being detected. Mathematically speaking, if $N_{E,i}$ signals are expected to be detected along the ith drift track, then the calculation of the number of passing events (tracks) that are detected, N_{PED}, involves a highly nonlinear operator

$$N_{\mathrm{PED}} = \mathrm{nint}\left(\sum_i \min(N_{E,i}) \right). \tag{9}$$

So, including fluctuations, $N'_{E,i}$, will change the outcome. Thus, $\rho(r, s_{\mathrm{ca}})$ is not sufficient in and of itself to calculate whether or not a passing event is expected to be detected and will tend to overestimate the number of passing events that are detected.

3.7. LTD Tracks and FVCOM Current

LTD tracks mostly pass near the middle of Minas Passage. Figure 8 shows a quasi-steady track (black) that passes repeatedly through the mid-channel of Minas Passage when

tides are running fast. Other quasi-steady trajectories have been identified [14], but they are of less interest to the present project because either they do not enter Minas Passage or they arrive at the study site near the low-water slack tide. Tracks that pass through the TED area have more variable trajectories over subsequent tidal cycles, as shown by the orange trajectory in Figure 8 and as reported for other trajectories [14]. As a result, LTDs are mostly suited for measuring how well passing events are detected to the south of the TED area.

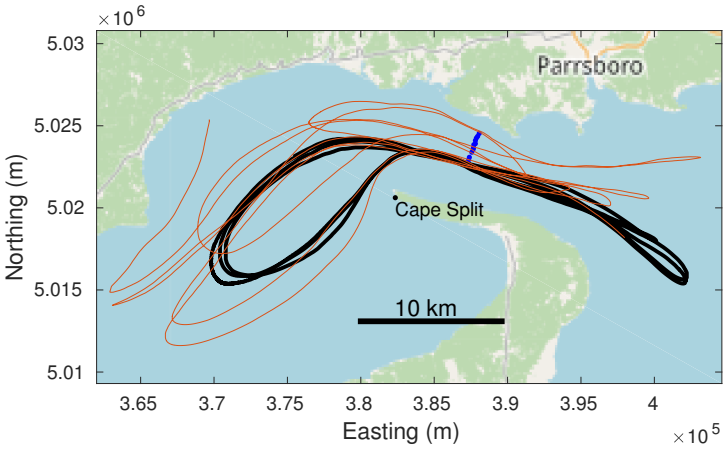

Figure 8. Two LTD tracks. A quasi-steady track (black) frequently passes near the southern end of the line of moored receivers (blue). A highly variable track (orange) sometimes passes through the northern end of the receiver line.

For the present analysis, we will only be concerned with the LTD passing events that crossed an extended line through the array of HR2 receivers. Sometimes, an LTD crossed the line, but GPS position measurements were too infrequent for accurate analysis. Of the remaining LTD passing events, 103 were measured on the flood tide and 114 on the ebb tide (Figure 9). Each LTD carried four tags, and the receiver array detected at least one of those tags for 81 passing events on the flood tide and 57 on the ebb tide. These detected passing events are colored blue in Figure 9. On the flood tide, centrifugal effects associated with inflow around Cape Split [14] tend to cause passing events to be distributed more to the north than during ebb tides (Figure 9).

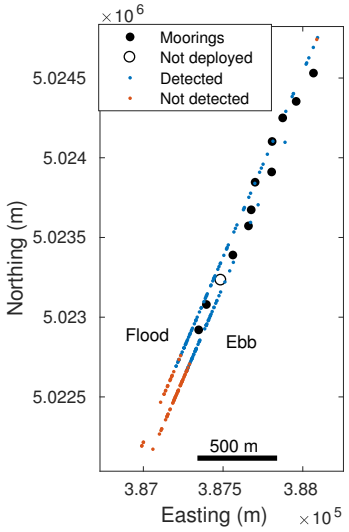

Figure 9. Dots indicate where LTD tracks crossed the mooring line, with flood crossings displaced to the left and ebb crossings displaced to the right. Blue dots indicate passing events that were detected by the array of HR2 receivers and orange dots indicate passing events that were not detected.

Figure 10 compares signed current speeds, s_{ca}, obtained at LTD passing events south of mooring 6 with the corresponding values of s_{FV} obtained from the FVCOM simulation. In the TED area, FVCOM underestimated STD current speed by about 13% (1), whereas in deeper waters to the south, FVCOM underestimates LTD current speed by about 24%. Some of this difference may be attributable to the LTD being drogue at about 6.3 m depth.

The energy-containing turbulent eddies are not resolved by FVCOM but they are a part of the drifter motion so they are expected to appear within the residuals in Figure 10. It is particularly noticeable that residuals show much more scatter about the fitted line on the flood tide than on the ebb tide (Figure 10). On the ebb tide, the mid-channel current is well collimated, whereas on the flood tide, there is substantial cross-channel movement associated with a strongly rotational flow around Cape Split (Figure 8). Turbulence is expected to be less in a collimated flow than in a strongly rotational flow, consistent with the pattern of residuals.

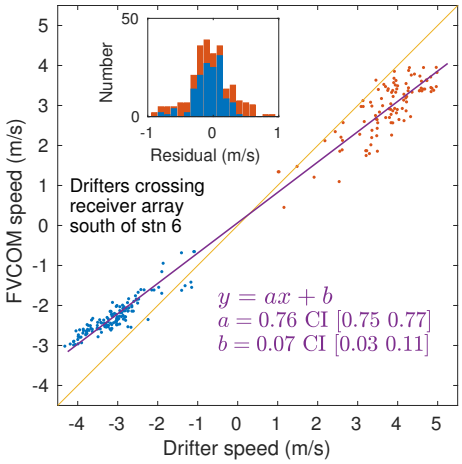

Figure 10. For each crossing that is south of mooring 6, the signed speed of the drifter, s_{ca}, is compared with the value obtained from the FVCOM model. A best-fit linear regression is plotted (purple).

3.8. Number of LTD Passing Events Detected by the Receiver Array

When a tagged fish is detected, we know that it has passed by our receivers, but we have no way to know how many times it passed by *without* the tag being detected. On the other hand, a GPS logger shows when a tagged drifter passed by receivers regardless of whether or not the tag is detected. The blue dots in Figure 9 show 138 LTD tracks had at least one tag detected while passing within (or nearby) the HR2 array.

Of course, each LTD carried four HR tags at different depths, so the 4×138 tag-passing events should be examined before drawing quantitative conclusions about how well a tagged fish might have been detected by such an array. Analysis for this question begins by excluding those passing events that were undetected (orange dots in Figure 9) because these were simply beyond the area over which the array can monitor. It is generally understood that passing events are more likely to be detected when current speed is slow, and it should not be assumed that the detection of passing events on a flood tide will be the same as on an ebb tide. This suggests four categories to investigate: slow flood, slow ebb, fast flood, and fast ebb.

The LTD passed the array 45 times on a fast flood tide, $s_{ca} > 3.5$ ms^{-1}. Counting the number of passing events for which the array detected a specified tag at least once gives the number of detected passing events for that tag, as shown in the top row of Table 5. None of the tags were detected on all 45 passing events, but 92% of the 4×45 tag-passing events were detected, and tags at different depths were detected similarly. Doubling the interval between transmissions (i.e., $\tau = 4$ s) did not change the number of detected passing events. Greater increases in τ reduced the number of detected passing events, and this reduction was always a little more for the near-surface (2.25 m) tag.

Table 5. Out of 45 fast flood-tide ($s_{ca} > 3.5$ ms^{-1}) LTD passing events, we tabulated the number of passing events for which tags at different depths were detected by the HR2 array. Dependence on increasing transmission interval, τ, was calculated.

τ (s)	2.25 m Tag	9 m Tag	19 m Tag	28 m Tag
2	41	42	40	42
4	41	42	40	42
8	40	41	39	40
16	35	39	37	37
32	28	34	34	31
64	18	26	27	21

Each tag was detected during 35 of the 36 slow flood passing events (Table 6). Clearly, if a tag was detected during a passing event, then it was typically detected many times because greatly increasing the interval between transmissions only caused a modest decline in the number of detected passing events. This is generally consistent with Figure 4, which shows many more detected signals for a lower speed passing event than for a faster passing event, even though the faster event more closely approached a moored receiver.

Table 6. Out of 36 slow flood-tide ($0 < s_{ca} \leq 3.5$ ms^{-1}) LTD passing events, we tabulated the number of passing events for which tags at different depths were detected by the HR2 array. Dependence on increasing transmission interval, τ, was calculated.

τ (s)	2.25 m Tag	9 m Tag	19 m Tag	28 m Tag
2	35	35	35	35
4	35	35	35	35
8	34	34	35	34
16	33	33	34	34
32	32	32	33	33
64	28	31	31	31

Ebb tide passing events (Tables 7 and 8) show similar trends to those of the flood tide (Tables 5 and 6). Generally, most tag-passing events were detected, and when compared to the STD passing events, they were also detected relatively well for moderately increased τ. Furthermore, it seems that signals reflected from the sea surface did not disrupt detection of near-surface tags for the LTD, although they did for the STD (Table 3). Many of the LTDs were detected by receivers moored at greater depths than those that detected the STD (Figure 1). All else being equal, (3) shows that the time lag between the direct signal and its reflection will be greater for a receiver at greater depths, but this is partly offset by the top tag being nearer the sea surface during the LTD, and the overall effect is not so great as to avoid interference. Previous work found that reflected signals were more likely to be detected in shallow than in deep water [13], so this might reduce interference for the near-surface tags of the LTD. Reflected signals are also less likely to be detected as significant wave height increases [13], and we note that calm conditions were selected for the STD, whereas LTD spanned a range of weather conditions.

Table 7. Out of 13 fast ebb tide ($s_{ca} < -3.5$ ms^{-1}) LTD passing events, we tabulated the number of passing events for which tags at different depths were detected by the HR2 array. Dependence on increasing transmission interval, τ, was calculated.

τ (s)	2.25 m Tag	9 m Tag	19 m Tag	28 m Tag
2	9	11	12	13
4	9	11	12	13
8	9	10	12	12
16	8	10	11	11
32	8	9	10	9
64	5	7	7	7

Table 8. Out of 44 slow ebb tide ($0 > s_{ca} \geq -3.5$ ms^{-1}) LTD passing events, we tabulated the number of passing events for which tags at different depths were detected by the HR2 array. Dependence on increasing transmission interval, τ, was calculated.

τ (s)	2.25 m Tag	9 m Tag	19 m Tag	28 m Tag
2	38	39	44	39
4	38	39	43	39
8	37	38	40	37
16	34	36	38	36
32	30	33	35	35
64	25	30	31	30

3.9. Number of HR Signals Detected by a Receiver during an LTD Passing Event

In order to use the telemetry measurements to calculate the probability of fish–turbine encounter, we could consider a moored HR2 receiver as a proxy for an MHK turbine and obtain the probability that a tagged fish would pass within a distance of the receiver that is commensurate with the projected frontal area, A_{MHK}, that the blades of an MHK turbine would sweep. Before studying tagged fish in our next paper [20], we presently use tags on drifters to evaluate whether or not a receiver detects a tag as it passes by at some range, r_{ca}, and speed, s_{ca}, at closest approach. HR2 receivers at moorings 1, 2, 4–7, and 9–10 showed no evidence of being moved, and mooring 8 did not move much. Let us, therefore, consider how receivers 1, 2, and 4–10 detected tags at 19 m and 28 m depth on the LTD.

In the TED area, Eulerian measurements of detection efficiency, ρ, did not have flood–ebb symmetry with respect to modeled tidal current, so ρ was represented as a function of signed speed, s_{FV}. The LTD provides an accurate current measurement, s_{ca}, at the time of a passing event, whereas currents from FVCOM simulations differ in various ways (Figure 10). For the LTD measurements, we found that N_D had flood–ebb symmetry with respect to measured currents and could be represented as a function of $|s_{ca}|$. It is unclear how well this symmetry in N_D applies to the TED area because the LTD mostly crossed the mooring line to the south of the TED area.

Given flood/ebb symmetry, Figure 11 groups measurements according to current speed, $|s_{ca}|$, and $\sqrt{N_D}$ is plotted as a function of r_{ca}. For $N_D > 0$, r_{ca} declines linearly with respect to $\sqrt{N_D}$. A best linear fit of $\sqrt{N_D}$ to r_{ca} was obtained for each speed group, as documented in the figure. Having measured a value of N_D from a tag on an LTD that passes by at a time when the current is within one of the plotted speed groups, the fitted equations in Figure 11 enable an estimate of its range of closest approach and the variation about that range. Similarly, evaluating r_{ca} for $N_D = 1/2$ gives a typical minimum range, λ_{LTD}, for the transition from a tag on a passing LTD being detected or not detected. λ is a key metric for calculating the probability of encounter [20].

The LTD measurements can be used to obtain the probability, p_{PED}, that a passing event will be detected by identifying which of the tag-LTD-passing events were detected by an HR2 receiver at r_{ca} and $|s_{ca}|$. Each tag-passing event is marked by a dot in Figure 12, with blue dots indicating a tag-passing event that is detected (i.e., $N_D \geq 1$) and red dots indicating an undetected tag-passing event. For each $(r_{ca}, |s_{ca}|)$ bin, p_{PED} is the ratio of the number of blue dots to the number of red and blue dots. Thus, for each range–speed bin, we enumerate the percentage of tag-passing events ($100 \times p_{PED}$) that were detected in each speed-range bin of Figure 12. Repeating this exercise for the tags at 2.25 m and 9 m depth gave a similar result. For all current speeds measured by the LTD, there is an 84–100% chance that an LTD track will be detected, providing it comes within $r_{ca} < 150$ m of a moored HR2 receiver.

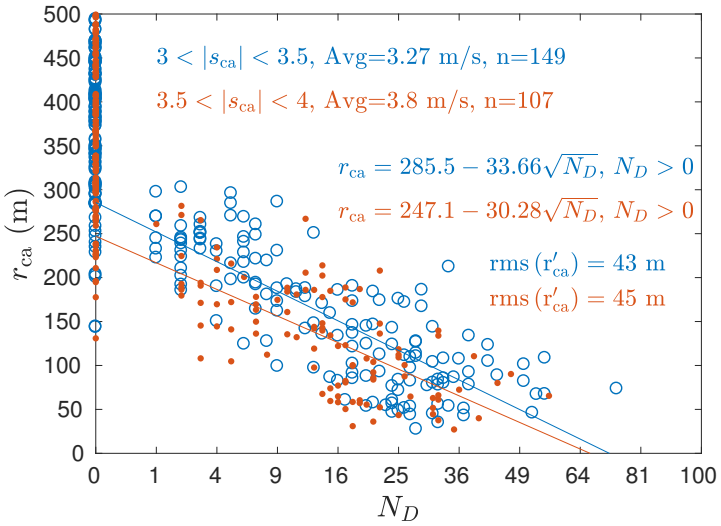

Figure 11. Relating the number of HR signals detected during am LTD passing event, N_D, to the range at closest approach, r_{ca}, for measurements grouped according to the speed at closest approach, $|s_{ca}|$. Each HR tag transmitted every $\tau = 2$ s.

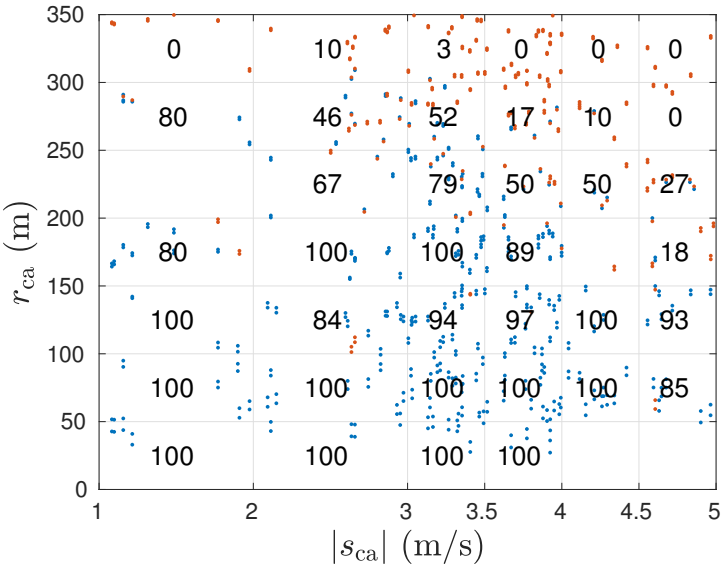

Figure 12. Percentage of tag-passing events that are detected by a moored HR2 receiver as a function of speed, $|s_{ca}|$, and range, r_{ca}, at closest approach. Here, we consider LTD of the two deepest HR tags (19 m and 28 m). Each tag transmitted every $\tau = 2$ s.

Figure 12 was obtained using HR tags that transmit every $\tau = 2$ s. The ith dot in Figure 12 represents a passing event for which the number of detected signals, N_{Di}, can be transformed following (4) in order to estimate how well tags are detected when fish carry tags with some larger transmission interval, T. Note that tagged-drifter experiments should use tags with small τ because (4) requires $T \geq \tau$.

3.10. LTD Comparison of HR and 69 kHz PPM

Two of the LTDs suspended a 69 kHz PPM tag (transmission interval 20 to 30 s) that was 0.5 m below the bottom HR tag (i.e., 28.5 m). For these two LTDs, we identified all tracks in which any of the five tags (four HR tags and a PPM tag) were detected. Table 9 compares the number of tracks for which the bottom HR tag was detected with the number of tracks for which the 69 kHz PPM tag was detected. Both tags were well detected at low current speed, with the 69 kHz PPM tag being detected on a few of the tracks where the

distance to a receiver was beyond the range of HR tags (Figure 9). At higher current speeds, the HR tag was much more reliable for detecting passing events.

Table 9. Number of LTD tracks for which the bottom HR and 69 kHz PPM tag were detected. Tracks are categorized according to whether the current is fast or slow on the ebb or flood tide.

# Tracks	HR Tag	PPM Tag	Current (ms^{-1})	Mean Current (ms^{-1})
28	27	28	$0 < s_{ca} < 3.5$	2.84
35	25	29	$0 > s_{ca} > -3.5$	−2.8
35	34	19	$s_{ca} > 3.5$	4.17
11	11	1	$s_{ca} < -3.5$	−3.8

4. Discussion

Using efficient MHK turbines [25] to harvest tidal energy at locations with high power density [4] is a state-of-the-art undertaking, but less intensive use of tidal energy is not a new thing [26]. Humans have exploited the energy of a turning tide ever since they began to use fishing weirs and marine craft [27]. The basic principle of a fishing weir is to collect fish that would otherwise pass by with the tide, and this is a conceptual starting point for quantifying an upper bound on the number of fish that might interact with an operating MHK turbine in Minas Passage.

If one were to replace the MHK turbine with a net that spans the same cross-current area, A_{MHK}, swept by the turbine blades, then the fish caught could be considered to approximate the number of individuals (belonging to captured species) that might pass through the operating turbine. Ecologists have similarly attempted to use active hydroacoustic devices to monitor backscatter from targets in a water volume similar to that which fluxes through A_{MHK}, but it has not proven possible to enumerate individuals or identify species from the backscatter observed in Minas Passage [18]. Optical cameras provide much higher resolution [28], and visibility may be sufficient in Minas Passage for cameras to identify a subset of those fish that an active hydroacoustic device detected upstream as backscatter.

It would be most useful if the above Eulerian methods successfully measured the number of individuals (for some species) that might encounter a MHK turbine, but this would still leave outstanding issues. From a population point of view, what matters is not so much the number that encounters an MHK turbine, but rather the proportion of a local population that encounters an MHK turbine. This proportion is difficult to calculate from catch/backscatter numbers because the local population number is not known for any of the species captured [9]. Furthermore, sometimes two fish belonging to the same species may belong to different populations [11]. Such difficulties can be resolved by using acoustic tags [10,11] to track individuals belonging to a known population, which amounts to measuring in the Lagrangian frame [15]. Tagging studies have been published for striped bass of Shubenacadie River origin [10]; Atlantic sturgeon that mostly originate from the Saint John River, New Brunswick [11]; and alewife of the Gaspereau River stock [29]. Lagrangian methods provide population-specific information that augments the previously discussed Eulerian methods that attempt to count all fish that pass through A_{MHK}.

It was hoped that probabilities of fish–turbine encounters could be calculated from measurements of striped bass [10] and Atlantic sturgeon [11] that carried 69 kHz PPM tags. Such calculations require estimates of detection efficiency in order to transform detected signals into estimates of abundance or a probability distribution of distance from the detecting receiver [13]. Detection range testing in Minas Passage [24] showed poor detection efficiency for 69 kHz PPM tags when current speed was fast. Another study [30] found that sturgeons carrying 69 kHz PPM tags were seldom detected in Minas Passage when the current was fast. The present results confirm that fish carrying 69 kHz PPM tags are unlikely to be detected by the receiver array in fast currents and yet will be detected by many receivers in the array when the current is slow. For estimating the probability of encounter, being detected over too wide an area causes uncertainty and not being detected

biases values low in fast currents for which a fish–turbine encounter is more likely to be harmful.

These shortcomings of PPM tags motivated the use of HR tags to track fish passing through the TED area in Minas Passage. Alewives carrying HR tags were detected at the TED area during a range of flood and ebb current conditions [29], which supports further consideration of HR tags. Detection range measurements [13] show that the HR signals are better detected than PPM signals in fast currents. A single PPM signal extends over an interval >2 s, whereas an HR signal takes only 6 ms, so it is possible to transmit a great many more HR signals, which gives more chances for an HR tag to be detected (6). The present work quantifies how a higher transmission rate makes it more likely that a drifter carrying an HR tag (a proxy for a tagged fish) will be detected by fixed receivers (Table 3).

When a PPM signal is reflected from the sea surface [13], it can cause close proximity detection interference [22] and prevent a nearby PPM tag from being detected. We observe that there are also geometric configurations of tag and receiver for which an HR signal overlaps with its reflection from the sea surface (3), but this only happens for a narrow set of circumstances, mostly when the tag is very near the sea surface and the sea surface is calm (Table 3). Under slightly different geometric circumstances, the reflected signal will not overlap with that taking a direct path, so the HR2 receiver has a second opportunity to detect the one HR transmission. Reflected signals are less likely to be observed, and less likely to cause interference, when the sea surface is rougher ([13], Table 5).

Another concern about both HR and PPM signal propagation was that previous detection range experiments [13,24] placed both receiver and acoustic tags close to the seafloor so that signals might sometimes be blocked by variable bathymetry. These previous experiments could not unambiguously identify where signal paths were blocked. The present mooring layout (Figure 1b) affords one obviously blocked path (mooring 9 to 10) plus a matching clear path (mooring 9 to 8), and the results demonstrate that detection efficiency is profoundly diminished for the blocked signal path (Figure 5). This justifies a decision to reject paths along which signal detection was poor in order to obtain an estimate for the detection efficiency, ρ, that applies to tagged fish that swim well clear of the seafloor [13].

Detection efficiency, ρ, is usually measured in the Eulerian frame, with both acoustic tag and receiver being at fixed coordinates relative to the seafloor [13,21,24]. On the other hand, a tagged fish is naturally described in a Lagrangian frame [15], as defined by its position at some initial time and subsequent trajectory due to movement by tidal current and swimming behavior. To achieve a robust estimate for the probability of fish–turbine encounters, we need to quantify that a fish carrying an HR tag will be detected as it passes over an array of HR2 receivers that monitor the TED area. Equation (6) relates the Eulerian detection efficiency, ρ, [13] to the number of times an HR signal is expected to be detected from a tagged fish (Lagrangian) as it passes a moored receiver. Given that ρ tended to overestimate the number of detection-positive intervals [13], the presently reported experiments were deemed necessary to directly measure how many times a fixed receiver detects a drifting tag as it passes by. Equation (6) was found to overestimate the number of passing trajectories for which there was at least one detected signal, and this overestimation can be attributed to the autocorrelation of variability about the general functional form of ρ. Nevertheless, most of the HR tags that drifters carried through the HR2 receiver array were detected, even during spring flood tides when current speeds were near their greatest extent in the TED area. Sometimes a passing tag was detected only a small number of times, so there was little margin for error. Indeed, the HR tags transmitted every 1.8 to 2.2 s, and if they had transmitted at longer intervals, then more tags would have passed by without being detected. A tagged fish that actively swims in the same sense as the tidal current may be somewhat less likely to be detected than a tagged fish drifting with the current [14].

The issue of tagged fish passing through a receiver array without being detected is also central to studies that use a sequence of receiver arrays to measure migration and

mortality/loss of tagged fish [29,31,32]. When fish are migrating, it is often possible to utilize detections of the tagged fish to roughly estimate detection efficiencies of most receiver arrays along the migration route, except for the last array [29,32]. It is very desirable, therefore, that the last array be designed so that it will detect all migrating fish as they pass by. The above work shows that detection range measurements are useful for obtaining a first estimate of the probability that the migrating fish will be detected by an array, but this estimate will be biased a little high.

A total of four HR2 receivers were used to monitor the TED area during this experiment. Although this was sufficient to detect the majority of HR tags passing by on drifters, the number of signals detected during a passing event was often small when tidal currents were greatest. It would be better to have had more HR2 receivers monitoring the TED area in order to (1) provide some redundancy in case of instrument failure, (2) better ensure that every tagged fish would be detected as it passed by, and (3) increase the possibility of localizing the position of a passing tag when several receivers detect the same HR signal. Localization does not have to be perfect, but it would be very helpful to know if tagged fish passed directly over the TED area or a little to the north or south.

Additionally, it would be advantageous to have a mooring system that enables HR2 receivers to be held sufficiently off the seafloor so as to prevent signals from one HR2 from being blocked before they reached a neighboring HR2. If this could be achieved, then HR detection efficiency could be accurately monitored as a function of time throughout the period when tagged fish are also being monitored. Rather than only relying on a fitted function for detection efficiency, $\rho(r, s_{\mathrm{FV}})$, it would be advantageous to also have a direct measurement of detection efficiency for the minute before and after a tagged fish is actually detected.

5. Conclusions

1. The present work clearly demonstrates that variable bathymetry can block HR signals. It follows that the omission of apparently blocked signal paths was justified in a previous study [13] that measured detection efficiency.
2. Detection efficiency is effectively 1 for HR signals transmitted from a ≈1 m range. This applies to all current speeds found in the TED area.
3. There is a reduced probability of HR signal detection when the tag drifts sufficiently near the sea surface for the reflection to interfere with the signal taking a direct path. Under calm conditions, this is expected to degrade the efficacy of HR telemetry for species of fish that swim near the sea surface.
4. The transmission interval between tag signals should be as short as practicable in order to minimize the chances that a drifting tag passes over the receiver array without being detected. With a transmission interval of 2 s, the receiver array at the TED area typically detected more than 90% of the deeper HR tags that drifted by when current speed was greater than 3.5 ms^{-1}.
5. Current speeds from the drifter tracks were larger than those from the FVCOM model.
6. Current speed has flood–ebb symmetry to the south of the TED area, but within the TED area, the flood current is much faster than the ebb.
7. The number of signals detected when LTD tags crossed the receiver array had flood–ebb symmetry with respect to drifter speed, whereas detection efficiency measured at the TED [13] does not have flood–ebb symmetry with respect to the current speed obtained from the FVCOM.
8. In fast currents, the number of signals detected from a tag that drifts by a fixed receiver was found to be slightly overestimated by integrating the Eulerian detection efficiency over the drift track. This effect might be attributed to correlated fluctuations in detection efficiency.
9. Drifter measurements have been used to tabulate the number of signals detected from a passing drifter as a function of current speed and the range of closest approach. This

can be considered a Lagrangian analog to an Eulerian detection efficiency, and subsequent work [20] shows how it is related to the probability of fish–turbine encounters.

10. The presently obtained results demonstrate how the previously measured detection efficiency, $\rho(r, s_{FV})$, [13] is related to the number of signals detected from a drifting tag when it passes over an array of receivers in the TED area. It, therefore, becomes possible to calculate the probability of fish–turbine encounters when the receiver array detects tagged fish as they pass through the TED area [20].

Author Contributions: Conceptualization, B.G.S. and D.J.H.; methodology, B.G.S. and D.J.H.; software, B.G.S.; validation, B.G.S.; formal analysis, B.G.S. and R.H.K.; investigation, B.G.S. and D.J.H.; resources, D.J.H. and B.G.S.; data curation, B.G.S.; writing—original draft preparation, B.G.S.; writing—review and editing, B.G.S., R.H.K. and D.J.H.; visualization, B.G.S.; supervision, B.G.S. and D.J.H.; project administration, D.J.H. and B.G.S.; funding acquisition, D.J.H. and B.G.S. All authors have read and agreed to the published version of this manuscript.

Funding: This research was funded by Natural Resources Canada (grant number: ERPP-RA-07).

Institutional Review Board Statement: Not applicable.

Informed Consent Statement: Not applicable.

Data Availability Statement: The data sets analyzed during the current study are available from the corresponding author upon reasonable request.

Acknowledgments: The Acadia Centre for Estuarine Research helped fund drifter experiments and provided laboratory space and equipment. Randy Corcoran assisted with the deployment and recovery of drifters. Shaun Allain improved the instrument configuration for moorings and prepared moorings. Moorings were deployed and recovered by Shaun Allain with the assistance of Mike Huntley and the crew of the Nova Endeavour.

Conflicts of Interest: The authors declare no conflict of interest. The funders had no role in the design of the study; in the collection, analyses, or interpretation of data; in the writing of the manuscript; or in the decision to publish the results.

Abbreviations

The following abbreviations are used in this manuscript:

FORCE	Fundy Ocean Research Centre for Energy
MHK	Marine Hydrokinetic
TED	Tidal Energy Development
PPM	Pulse-Position Modulation
HR	High Residency
HR2	High Residence Receiver
CI	Confidence Interval
UTC	Coordinated Universal Time
FVCOM	Finite-Volume Coastal Ocean Model
ABS	Acrylonitrile–Butadiene–Styrene
LTE	Long-Term Evolution
DC	Direct Current
USB	Universal Serial Bus
STD	Short-Term Drifts
LTD	Long-Term Drifts
GPS	Global Positioning System

References

1. Copping, A.; Hemery, L. (Eds.) *OES-Environmental 2020 State of the Science Report: Environmental Effects of Marine Renewable Energy Development Around the World*; Report for Ocean Energy Systems (OES); Office of Scientific and Technical Information: Oak Ridge, TN, USA, 2020. [CrossRef]
2. Jeffcoate, P.; McDowell, J. Performance of PLAT-I, a floating tidal energy platform for inshore applications. In Proceedings of the 12th European Wave and Tidal Energy Conference, Cork, Ireland, 27 August–1 September 2017.

3. Murray, J. Evolution of a solution for low cost tidal stream energy. *J. Ocean. Technol.* **2021**, *16*, 1–8.
4. Karsten, R.; McMillan, J.; Lickley, M.; Haynes, R. Assessment of tidal current energy in the Minas Passage, Bay of Fundy. *J. Power Energy* **2008**, *222*, 289–297. [CrossRef]
5. Karsten, R. An assessment of the potential of tidal power from Minas Passage, Bay of Fundy, using three-dimensional models. In Proceedings of the ASME 2001 30th International Conference on Ocean, Offshore and Arctic Engineering, OMEA2011-49249, Rotterdam, The Netherlands, 19–24 June 2011.
6. Bangley, C.W.; Hasselman, D.J.; Flemming, J.M.; Whoriskey, F.G.; Culina, J.; Enders, L.; Bradford, R.G. Modeling the Probability of Overlap Between Marine Fish Distributions and Marine Renewable Energy Infrastructure Using Acoustic Telemetry Data. *Front. Mar. Sci.* **2022**, *9*, 851757. [CrossRef]
7. Dadswell, M.J.; Wehrell, S.A.; Spares, A.D.; Mclean, M.F.; Beardsall, J.W.; Logan-Chesney, L.M.; Nau, G.S.; Ceapa, C.; Redden, A.M.; Stokesbury, M.J. The annual marine feeding aggregation of Atlantic sturgeon Acipenser oxyrinchus in the inner Bay of Fundy: population characteristics and movement. *J. Fish Biol.* **2016**, *89*, 2107–2132. [CrossRef]
8. Dadswell, M.J.; Spares, A.D.; McLean, M.F.; Harris, P.J.; Rulifon, R.A. Long-term effect of a tidal, hydroelectric propeller turbine on the populations of three anadromous fish species. *J. Fish Biol.* **2018**, *93*, 192–206. [CrossRef]
9. Dadswell, M.J.; Spares, A.D.; Porter, E.; Porter, D. Diversity, abundance and size structure of fishes and invertebreates captured by an intertidal fishing weir at Bramber, Minas Basin, Nove Scotia. *Proc. Nova Scotia Inst. Sci.* **2020**, *50*, 283–318.
10. Keyser, F.; Redden, A.M.; Sanderson, B.G. Winter presence and temperature-related diel vertical migration of Striped Bass *Morone saxatilis* in an extreme high flow passage in the inner Bay of Fundy. *Can. J. Fish. Aquat. Sci.* **2016**, *73*, 1777–1786. [CrossRef]
11. Stokesbury, M.J.W.; Logan-Chesney, L.M.; McLean, M.F.; Buhariwalla, F.F.; Redden, A.M.; Beardsall, J.W.; Broome, J.; Dadswell, M.J. Atlantic sturgeon spatial and temporal distribution in Minas Passage, Nova Scotia: A region of future tidal power extraction. *PLoS ONE* **2016**, *11*, e0158387. [CrossRef]
12. DFO. *Recovery Potential Assessment for Inner Bay of Fundy Atlantic Salmon*; DFO Canadian Science Advisory Secretariat Science Advisory Report 2008/050; Centre for Science Advice (CSA), Maritimes Region, Department of Fisheries and Oceans: Dartmouth, NS, Canada, 2008.
13. Sanderson, B.G.; Bangley, C.W.; McGarry, L.P.; Hasselman, D.J. Measuring detection efficiency of 170 kHz high-residency acoustic signals in a fast-flowing tidal passage. *J. Mar. Sci. Eng.* **2023**, *11*, 1172. [CrossRef]
14. Sanderson, B.G.; Stokesbury, M.J.W.; Redden, A.M. Using trajectories through a tidal energy development site in the Bay of Fundy to study interaction of renewable energy with fish. *J. Ocean Technol.* **2021**, *16*, 50–70.
15. Neumann, G.; Pierson, W. *Principles of Physical Oceanography*; Prentice-Hall Inc.: Englewood Cliffs, NJ, USA, 1966; pp. 1–545.
16. Viehman, H.A.; Zydlewski, G.B. Fish Interactions with a Commercial-Scale Tidal Energy Device in the Natural Environment. *Estuaries Coasts* **2015**, *38* (Suppl. S1), S214–S252. [CrossRef]
17. Amaral, S.V.; Bevelhimer, M.S.; Cada, G.F.; Giza, D.J.; Jacobson, P.T.; McMahon, B.J.; Pracheil, B.M. Evaluation of behavior and survival of fish exposed to an axial-flow hydrokinetic turbine. *N. Am. J. Fish. Manag.* **2015**, *35*, 97–113. [CrossRef]
18. Viehman, H.A.; Hasselman, D.J.; Douglas, J.; Boucher, T. The ups and downs of using active acoustic technologies to study fish at tidal energy sites. *Front. Mar. Sci.* **2022**, *9*, 851400. [CrossRef]
19. Renkawitz, M.D.; Sheehan, T.F.; Goulette, G.S. Swimming depth, behavior, and survival of Atlantic salmon postsmolts in Penobscot Bay, Maine. *Trans. Am. Fish. Soc.* **2012**, *141*, 1219–1229. [CrossRef]
20. Sanderson, B.G.; Karsten, R.; Solda, C.; Hardie, D.C.; Hasselman, D.J. Probability of Atlantic salmon post-smolts encountering a tidal turbine installation in Minas Passage, Bay of Fundy. *J. Mar. Sci. Eng.* **2023**, *11*, 1095. [CrossRef]
21. Kessel, S.T.; Cooke, S.T.; Heupel, M.R.; Hussey, N.E.; Simpfendor, C.A.; Vagle, S.; Fisk, A.T. A review of detection range testing in aquatic passive acoustic telemetry studies. *Rev. Fish Biol. Fish.* **2014**, *24*, 199–218. [CrossRef]
22. Kessel, S.T.; Hussey, N.E.; Webber, D.M.; Gruber, S.H.; Young, J.M.; Smale, M.J.; Fisk, A.T. Close proximity detection interference with acoustic telemetry: The importance of considering tag power output in low ambient noise environments. *Anim. Biotelemetry* **2015**, *3*, 5. [CrossRef]
23. Chen, C.; Beardsley, R.C.; Cowles, G. An Unstructured-Grid, Finite-Volume Coastal Ocean Model (FVCOM) System. *Oceanography* **2006**, *19*, 78–89. [CrossRef]
24. Sanderson, B.G.; Buhariwalla, C.; Adams, M.; Broome, J.; Stokesbury, M.; Redden, A.M. Quantifying detection range of acoustic tags for probability of fish encountering MHK devices. In Proceedings of the 12th European Wave and Tidal Energy Conference, Cork, Ireland, 27 August–1 September 2017.
25. Betz, A. *Introduction to the Theory of Flow Machines*; Randall, D.G., Ed.; Pergamon Press: Oxford, UK, 1966.
26. Charlier, R.H.; Menanteay, L. The saga of tide mills. *Renew. Sustain. Energy Rev.* **1997**, *1*, 171–207. [CrossRef]
27. Pederson, L. 7000 years of fishing; stationary fishing structures in the Mesolithic and afterwards. In *Man and Sea in the Mesolithic*; Fisher, A., Ed.; Oxbow Books: Oxford, UK, 1995; pp. 75–86.
28. Hammar, L.; Andersson, S.; Eggertsen, L.; Haglund, J.; Gullstrom, M.; Ehnberg, J.; Molander, S. Hydrokinetic Turbine Effects on Fish Swimming Behaviour. *PLoS ONE* **2013**, *8*, e84141. [CrossRef]
29. Tsitrin, E.; Sanderson, B.G.; McLean, M.F.; Gibson, A.J.F.; Hardie, D.C.; Stokesbury, M.J.W. Migration and apparent survival of postspawning alewife (*Alosa pseudoharengus*) in Minas Basin, Bay of Fundy. *Anim. Biotelemetry* **2022**, *10*, 11. [CrossRef]
30. Lilly, J.; Dadswell, M.J.; Mclean, M.f.; Avery, T.S.; Comolli, P.D.; Stokesbury, M.J.W. Atlantic sturgeon presence in a designated marine hydrokinetic test site prior to turbine deployment: A baseline study. *J. Appl. Ichthyol.* **2021**, *37*, 826–834. [CrossRef]

31. Kocik, J.F.; Hawkes, J.P.; Sheehan, T.F.; Music, P.A.; Beland, K.F. Assessing Estuarine and Coastal Migration and Survival of Wild Atlantic Salmon Smolts from the Narraguagus River, Maine Using Ultrasonic Telemetry. *Am. Fish. Soc. Symp.* **2009**, *69*, 293–310.
32. Halfyard, E.A.; Gibson, A.J.; Ruzzante, D.E.; Stokesbury, M.J.; Whoriskey, F.G. Estuarine survival and migratory behaviour of Atlantic salmon *Salmo salar* smolts. *J. Fish. Biol.* **2012**, *81*, 1626–1645. [CrossRef] [PubMed]